Unique Aspects of the 1-Methylimidazole Ligation to Corrphycenatoiron(III)

Saburo Neya,* Yoshiki Ohgo, † Mikio Nakamura,† and Noriaki Funasaki

Department of Physical Chemistry, Kyoto Pharmaceutical University, Yamashina, Kyoto 607-8414

†Department of Chemistry, Toho University School of Medicine, Omorinishi, Ota-ku, Tokyo 143-8540

(Received July 12, 2000)

The coordination behaviors of chloro corrphycenatoiron(III), a novel hemin isomer with a trapezoidal metallo core, against imidazole, 1-methylimidazole, and 2-methylimidazole were followed by spectrophotometry in chloroform at room temperature. The examined compound is chloro 12,17-bis(ethoxycarbonyl)-2,3,6,7,11,18-hexamethylcorrphycenatoiron-(III). Titration of 2-methylimidazole and imidazole proceeded with and without accumulation of an intermediate mono imidazole species, respectively. On the other hand, a significant amount of an intermediate adduct was found to accumulate during 1-methylimidazole binding despite the absence of any steric hindrance in the iron(III)–*N*(1-methylimidazole) coordination bond. This is in remarkable contrast with the conventional results for porphyrinatoiron(III). The proton NMR analysis of the mono 1-methylimidazole binding to corrphycenatoiron(III) afforded a formation constant closely similar to that obtained from the visible spectra. EPR definitely assigned the iron(III) high-spin state for the intermediate. Accumulation of the mono 1-methylimidazole intermediate was explained in terms of the contracted core in corrphycene. The narrow iron cavity weakens the axial iron–chloride bond facilitating coordination of the first 1-methylimidazole. The four non-orthogonal iron(III)–*N*(pyrrole) bonds formed in the trapezoidal cavity further disturb the incoming motion of the iron(III) atom into corrphycene plane upon second 1-methylimidazole ligation. Accumulation of mono 1-methylimidazole intermediate was more evident in ferric corrphycenatoiron(III) with bromide and iodide, supporting the proposed changes in iron reactivity upon deformation of the equatorial coordination environment.

Porphyrinatoiron(III) is the essential constituent of heme-enzymes involved in a surprising number of vital processes. The versatility of porphyrin systems arises from its structural aspect to form complexes with iron and other various transition metals. The fundamental structure of porphyrin is characterized with a symmetrical array of cyclic tetrapyrrole. Rearrangement of the tetrapyrroles results in several types of novel porphyrin isomers with peculiar molecular shapes.[1] Corrphycene, an isomeric [18]porphyrin-(2.1.0.1), was independently prepared[2] in 1994 by the Sessler–Vogel groups and the Guilard laboratory. Falk et al.[3] and Neya et al.[4] designed other skillful synthetic routes. Corrphycene, like porphyrin, is a planar aromatic macrocycle.[1] Owing to the direct pyrrole–pyrrole link and the diagonal ethene bridge, the metallo core of corrphycene is trapezoidal, in remarkable contrast with the square hole of porphyrin. Corrphycene, despite the deformed and contracted central core, is capable of coordinating a variety of metal ions, and the iron complex of corrphycene has been prepared and characterized.[1c] The perceptible similarity of corrphycene to porphyrin suggests its possible utilization as a prosthetic group of hemoprotein. Neya et al.[5] introduced corrphycenatoiron(II) into the myoglobin pocket to analyze the binding of dioxygen and carbon monoxide. The myoglobin reconstitution was successfully carried out with corrphycenatoiron(III). Analysis of the imidazole ligation profile is important to quantitatively estimate the axial heme–globin interactions[6] in the reconstituted myoglobin and to explain the corrphycene introduction into protein matrix.

Axial coordination chemistry of corrphycenatoiron(III) still remains to be fully explored, while extensive results have already been accumulated for porphyrinatoiron(III).[7—15] Reactivity of the iron atom in a deformed porphyrin framework will be of considerable interest. In chloro corrphycenatoiron-(III), the iron atom is displaced from the plane just as in porphyrin.[1c,16] The displaced iron is expected to come into the corrphycene plane upon ligation of two imidazole molecules. Corrphycene with a constrained central core should influence dynamic motion of the chelating iron atom. We set out to examine the binding of imidazole (Im), 1-methylimidazole (1-MeIm), and 2-methylimidazole (2-MeIm) to the iron(III) complex of 12,17-bis(ethoxycarbonyl)-2,3,6,7,11,18-hexamethylcorrphycene (**1**) (Fig. 1). Comparison of this corrphycenatoiron(III) with the known synthetic[9,13—15] and natural[7,8,10,13] hemins, unfortunately, is not directly possible because of differences in solvent, temperature, concentration, and peripheral substituents. In this context, we also examined 13,17-diethoxycarbonyl-2,3,7,8,12,18-hexamethylporphyrinatoiron(III) (**2**), a close reference with the same peripheral substituents (Fig. 1). Different iron(III) reactivity between corrphycene and porphyrin, due to the equatorial coordination geometry, will be more directly evaluated with an intimate pair of molecules in Fig. 1. The detailed analysis of axial coordination chemistry of corrphycenatoiron(III) will

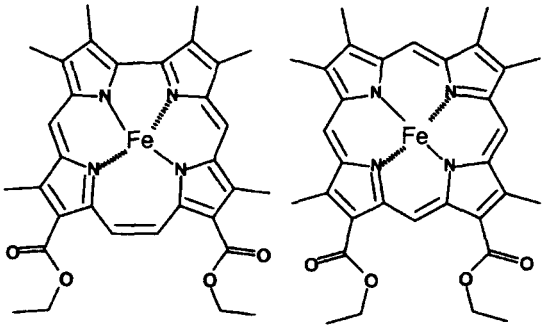

1 2

Fig. 1. Structure of the iron complexes of corrphycene (**1**) and porphyrin (**2**). A counter anion X (Cl^-, Br^-, or I^-) is attached to the iron(III).

be helpful to improve our understanding about the geometric control of metal reactivity by isomeric porphyrins.

Experimental

Materials. 12,17-Bis(ethoxycarbonyl)-2,3,6,7,11,18-hexamethylcorrphycene[4] and 12,17-bis(ethoxycarbonyl)-2,3,7,8,11,18-hexamethylporphyrin[17] were synthesized according to the reported methods. 12,17-Bis(ethoxycarbonyl)-11,18-dimethyl-2,3,6,7-tetraethylcorrphycene (*inset*, Fig. 6), a higher homologue, was prepared with the synthesis[4] by substituting 3,4-dimethylpyrrole with 3,4-diethylpyrrole. Anal. Calcd for $C_{36}H_{42}N_4O_4$: C, 72.70; H, 7.12; N, 9.42. Found: C, 71.55, H, 6.97; N, 9.33. ^{1}H NMR (300 MHz, $CDCl_3$) δ = 10.57 (s, 2H, -CH=CH-), 9.86 (s, 2H, -CH=), 4.83 (q, 4H, $-OC\underline{H}_2CH_3$), 3.99 (q, 2H, $-C\underline{H}_2CH_3$), 3.87 (q, 2H, $-C\underline{H}_2CH_3$), 3.73 (s, 6H, ring $-CH_3$), 1.81 (t, 6H, $-OCH_2C\underline{H}_3$), 1.73 (t, 6H, $-CH_2C\underline{H}_3$), 1.72 (t, 6H, $-CH_2C\underline{H}_3$). MS *m/z*, 595 (M+1). UV-vis (CH_2Cl_2), λ_{max} (10^{-3} ε, $M^{-1}cm^{-1}$): 418 (104), 516 (6.93), 552 (5.99), 577 (4.70), 628 nm (2.17), where 1 M = 1 mol dm^{-3}.

Iron was inserted to the free base after Adler et al.[19] to afford the chloro iron(III) complex. The bromo and iodo derivatives, prepared after cleavage of the oxo-bridged dimers[19] by dilute aqueous perchloric acid containing a saturating amount of corresponding sodium halide, were purified on silica-gel column with dichloromethane–methanol (98 : 2) as eluent before crystallization from dichloromethane-hexane. The identity of these complexes was optically checked. The UV-vis ($CHCl_3$) spectra are as follows: **1**·Cl, λ_{max} (10^{-3} ε, $M^{-1}cm^{-1}$): 399 (97.0), 490 (sh, 10.9), 510 (sh, 9.2), 540 (sh, 6.2), 638 (6.4); **1**·Br, 405 (92.0), 495 (sh, 11.5), 515 (sh, 9.6), 550 (sh, 5.7), 633 (5.2); **1**·I, 385 (sh, 80.7), 408 (90.0), 517 (12.1), 555 (sh, 9.0), 646 (5.0); **2**·Cl, 385 (70.8), 412 (76.0), 509(11.7), 540 (10.7), 640 (4.2); **2**·Br, 393 (81.0), 515 (10.8), 512 (9.8), 651 (3.9); **2**·I, 397 (90.0), 521 (13.8), 560 (sh, 13.3), 654 nm (4.1). The chemical shift analysis by ^{1}H NMR indicated that these complexes were at all times greater than 99% NMR pure.

Chloroform was dried with $CaCl_2$, distilled from CaH_2, and stored[20] in a brown bottle over molecular sieves. Imidazoles were available from Aldrich. Imidazole and 2-methylimidazole were twice recrystallized from benzene, and 1-methylimidazole, distilled from sodium hydroxide shortly before use, was stored in a closed bottle over molecular sieves.

Physical Measurements. Electronic absorption spectra were recorded on a Shimadzu-MPS 2000 spectrophotometer equipped with cell compartments maintained at 20±0.5 °C with circulating water bath. Proton nuclear magnetic resonance (NMR) spectra at 300 MHz were obtained at 20 °C on a Varian XL-300 apparatus with tetramethylsilane as an internal reference. Electron paramagnetic resonance (EPR) measurements were carried out on a Bruker ESP-300E X-band spectrometer operating at 9.458505 GHz and a microwave power of 1.02 mW under modulation frequency 100 kHz and modulation amplitude 7.58 Gauss. The spectra were obtained at 4 K with an Oxford helium cryostat.

Ligand Binding. Spectrophotometric titration on Shimadzu MPS-2000 was carried out with screw-capped cuvettes to prevent solvent evaporation during measurements. Small aliquots, 1—10 μl, of stock imidazole solution were added to the macrocycle, typically 10 μM in 3.5 ml chloroform, and the spectra were recorded after preliminary equilibration for three minutes. The iron concentrations for the proton NMR and EPR were 1.0 and 0.5 mM, respectively.

Results

Binding of Imidazole and 2-Methylimidazole.

Figure 2 shows the Soret absorption changes of chloro corrphycenatoiron(III) **1**·Cl upon addition of Im. The well-defined isosbestic points at 407 and 435 nm suggest that the equilibrium reflects the direct bis ligation. The changes were analyzed according to Eq. 1:

$$\mathbf{1}\cdot Cl + 2\ Im \rightleftarrows \mathbf{1}\cdot Im_2Cl \qquad \beta_2 = [\mathbf{1}\cdot Im_2Cl]/[\mathbf{1}\cdot Cl][Im]^2 \qquad (1)$$

The Hill plots[7] of $\log((A_0-A)/(A-A_2))$ vs. log [Im] afforded a straight line with slope $n = 1.97$ and an overall formation constant $\beta_2 = 6.0\times10^7$ M^{-2} (1 M = 1 mol dm^{-3}), where A_0 and A_2 refer to the absorbances for **1**·Cl and **1**·Im_2, respectively, and A is the observed absorbance in the presence of

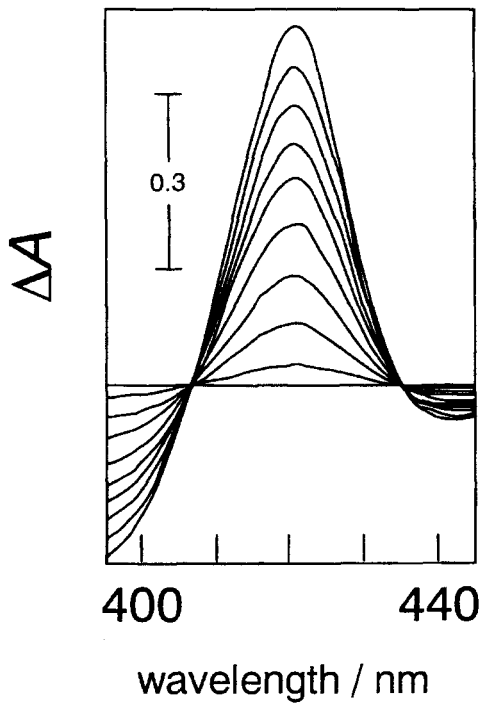

Fig. 2. Difference spectral changes in the Soret region during imidazole (Im) titration to **1**·Cl in $CHCl_3$ at 20 °C. The iron concentration is 11.0 μM, and Im increases from 0 to 8.81 mM.

a non-saturating amount of Im. The titration of Im to the corresponding porphyrin **2**·Cl, as also monitored in a Soret region, afforded $n = 1.95$ and $\beta_2 = 1.7\times10^7\ M^{-2}$.

When 2-MeIm, a typical "hindered" imidazole, was added to **1**·Cl, a sharp isosbestic point occurred at 411 nm below 3 mM of the ligand. At higher 2-MeIm concentrations of 25—55 mM, poorly intersecting isosbestic points were observed around 384 and 485 nm (results not shown). These two-step behaviors are consistent with the following stepwise 2-MeIm binding:

$$\mathbf{1}\text{·Cl} + \text{2-MeIm} \rightleftarrows \mathbf{1}\text{·2-MeIm·Cl}$$

$$K_1 = [\mathbf{1}\text{·2-MeIm·Cl}]/[\mathbf{1}\text{·Cl}][\text{2-MeIm}] \quad (2)$$

$$\mathbf{1}\text{·2-MeIm·Cl} + \text{2-MeIm} \rightleftarrows \mathbf{1}\text{·2-MeIm}_2\text{·Cl}$$

$$K_2 = [\mathbf{1}\text{·2-MeIm}_2\text{·Cl}]/[\mathbf{1}\text{·2-MeIm·Cl}][\text{2-MeIm}] \quad (3)$$

The first process, analyzed with the plots $1/(A_0 - A)$ vs. 1/[2-MeIm] after Benesi and Hildebrand,[21] afforded $K_1 = 710\ M^{-1}$. Application of the Benesi-Hildebrand equation to the second step was not possible because of the overlapping contribution of the first equilibrium, as evidenced by the ill-defined isosbestic points. The second process under the overlapping conditions was analyzed with the following equation:[22,23]

$$A = \frac{A_0 + A_1K_1[\text{2-MeIm}] + A_2K_1K_2[\text{2-MeIm}]^2}{1 + K_1[\text{2-MeIm}] + K_1K_2[\text{2-MeIm}]^2} \quad (4)$$

where A_i s ($i = 0$, 1, and 2) represent the absorbance of **1**·Cl coordinated with i 2-MeIm molecule(s), and A, the observed absorbance, is the weighted average of A_i s. With the K_1 and A_1 obtained from Eq. 2, K_2 and A_2 may be determined by rearranging Eq. 4 into Eq. 5:[22,23]

$$\frac{A - A_0}{A[\text{2-MeIm}]^2} + \frac{(A - A_0)K_1}{A[\text{2-MeIm}]} = K_1K_2A_2\frac{1}{A} - K_1K_2 \quad (5)$$

The values in $K_1K_2A_2$ and $-K_1K_2$ are resolved as the slope and intercept, respectively, of the linear plot of the left-hand side in Eq. 5 against $1/A$. Analysis of the 420-nm absorption changes with Eq. 5 afforded $K_2 = 2.1\ M^{-1}$ for **1**·Cl. The two-step 2-MeIm binding was also observed for corresponding porphyrin **2**·Cl. From the Soret absorption analyses according to Eqs. 2 and 3, we obtained $K_1 = 390\ M^{-1}$ and $K_2 = 40\ M^{-1}$ for **2**·Cl.

The above results are summarized in Table 1. Both the apparent absence of mono Im intermediate and the appreciable accumulation of mono 2-MeIm adduct agree with the results reported for a number of porphyrinatoiron(III) complexes,[7—9,12,14,15] suggesting a close similarity of corrphycene to porphyrin.

Binding of 1-Methylimidazole. Contrary to the above results for Im and 2-MeIm, the coordination behavior against 1-MeIm was remarkably different between **1**·Cl and **2**·Cl. The Soret absorption of **2**·Cl decreased at 377 nm and increased at 419 nm through an isosbestic point at 402 nm in a concentration range of 1-MeIm up to 100 mM. The 419-nm absorption changes followed Eq. 1 indicating non-appreciable accumulation of an intermediate. Analysis[7] afforded $\beta_2 = 2.88\times10^4\ M^{-2}$ for **2**·Cl, consistent with the direct bis coordination of 1-MeIm to tetraphenyl- and octaethyl-porphyrinatoiron(III) complexes.[9—13]

On the other hand, the coordination of 1-MeIm to **1**·Cl was remarkably distinct. As illustrated in Fig. 3, clear isosbestic points occurred at 402 and 453 nm below 0.7 mM 1-MeIm while the cross points are found around 406 and 418 nm above 5 mM 1-MeIm. These observations suggest the 1-MeIm binding in two steps. The optical changes were analyzed in Fig. 4 according to Eqs. 2 and 3 to afford $K_1 = 930\ M^{-1}$ and $K_2 = 290\ M^{-1}$ for **1**·Cl. The equilibrium constants are compiled in Table 1.

Proton Nuclear Magnetic Resonance. We examined proton NMR[24] to confirm the unique behavior of **1**·Cl against 1-MeIm. Figure 5 shows the spectral changes of **1**·Cl with increasing amounts of 1-MeIm. The three signals from six methyl groups, as expected from the two-fold symmetric corrphycene (Fig. 1), appeared at $\delta = 91.7$, 78.4, and 67.9 in the absence of 1-MeIm. The chemical shifts of these signals are dependent on the 1-MeIm concentration.[25] Incremental addition of 1-MeIm caused downfield shift of the 91.7-ppm signal, while the remaining two peaks exhibited upfield bias.

Table 1. Spectrophotometric Determination of Imidazole Affinities to the Iron(III) Derivatives of Corrphycene (**1**)[a] and Porphyrin (**2**)[a] in $CHCl_3$ at 20 °C

Macrocycles	Imidazoles[b]	K_1/M^{-1}	K_2/M^{-1}	β_2^{c}/M^{-2}
1·Cl	Im	—	—	$(6.03\pm0.38)\times10^7$
2·Cl	Im	—	—	$(1.68\pm0.12)\times10^7$
1·Cl	2-MeIm	705±5	2.10±0.30	$(1.48\pm0.22)\times10^3$
2·Cl	2-MeIm	386±18	40.0±5.1	$(1.54\pm0.27)\times10^4$
1·Cl	1-MeIm	934±56	294±17	$(2.75\pm0.33)\times10^5$
2·Cl	1-MeIm	—	—	$(2.88\pm0.23)\times10^4$
1·Br	1-MeIm	$(1.95\pm0.31)\times10^4$	4.10±0.79	$(8.00\pm2.81)\times10^4$
2·Br	1-MeIm	85.0±10.1	68.8±16.1	$(5.85\pm2.04)\times10^3$
1·I	1-MeIm	$(1.55\pm0.40)\times10^4$	6.51±2.61	$(1.01\pm0.66)\times10^5$
2·I	1-MeIm	$(2.00\pm0.57)\times10^3$	4.10±1.33	$(8.20\pm5.00)\times10^3$

a) Structure is given in Fig. 1. b) Abbreviations used: Im = imidazole; 1-MeIm, 1-methylimidazole; 2-MeIm, 2-methylimidazole.
c) Overall formation constant β_2 was calculated from K_1K_2 or experimentally determined in case of the direct bis coordination.

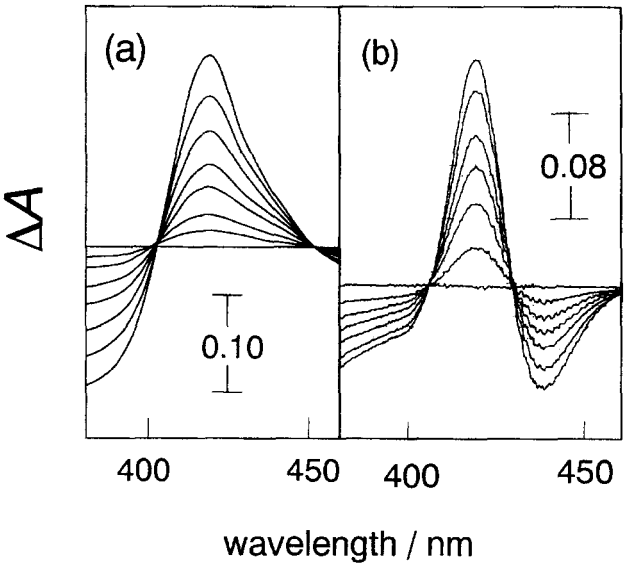

Fig. 3. (a) Optical absorption changes of **1**·Cl during 1-MeIm titration in $CHCl_3$ at 20 °C. The iron concentration is 11.1 μM, and 1-MeIm increases from 0 to 0.681 mM. (b) Soret difference spectra during 1-MeIm titration to **1**·Cl, 11.7 μM, in $CHCl_3$ at 20 °C. The base line was recorded at [1−MeIm] = 5.38 mM, and the final 1-MeIm concentration is 42.1 mM.

Above 2 mM of 1-MeIm, the methyl signals broadened out, accompanied with the appearance of one methyl peak at δ = 72.8 from the bis 1-MeIm adduct. At the high concentration extreme of 1-MeIm, only the 72.8-ppm signal of the bis adduct remained. Thus the changes proceeded in two steps. The concentration dependent shift in the first process was analyzed with the Benesi-Hildebrand equation modified for NMR analysis[26,27] under the fast exchange conditions:

$$\frac{1}{\delta_0 - \delta} = \frac{1}{K_1(\delta_0 - \delta_1)}\frac{1}{[\text{1-MeIm}]} + \frac{1}{\delta_0 - \delta_1} \qquad (6)$$

where δ_0 and δ_1 are the chemical shifts for **1**·Cl and the mono 1-MeIm complexes, respectively, and δ is the weighted average of δ_0 and δ_1. From the plots of $1/(\delta_0 - \delta)$ vs. 1/[1-MeIm] for the 67.9-ppm methyl peak in Fig. 5, we obtained $K_1 = 900\ M^{-1}$ for **1**·Cl. The K_1 is in good agreement with $K_1 = 930\ M^{-1}$ from the visible spectra in Fig. 3 despite a marked concentration increase in **1**·Cl for the NMR observation. On the other hand, the 1-MeIm binding to **2**·Cl revealed a single NMR transition. With addition of 1-MeIm, the heme methyl signals of **2**·Cl at δ = 55.0, 53.5, and 39.6 decreased in intensity, with concomitant appearance of the new methyl peaks at δ = 23.5, 20.7, and 13.0. Above 20 mM of 1-MeIm, only the new methyl peaks from the bis 1-MeIm complex of **2** remained. The process was slow on the NMR time scale, so that the chemical shifts of the methyl signals were invariant. The NMR results for **2**·Cl demonstrate the absence of an intermediate species.

Electron Spin Resonance. The 1-MeIm binding to chloro corrphycenatpiron(III) was examined by EPR to further confirm accumulation of the intermediate. We employed the tetraethyl compound (*inset*, Fig. 6), a higher homologue

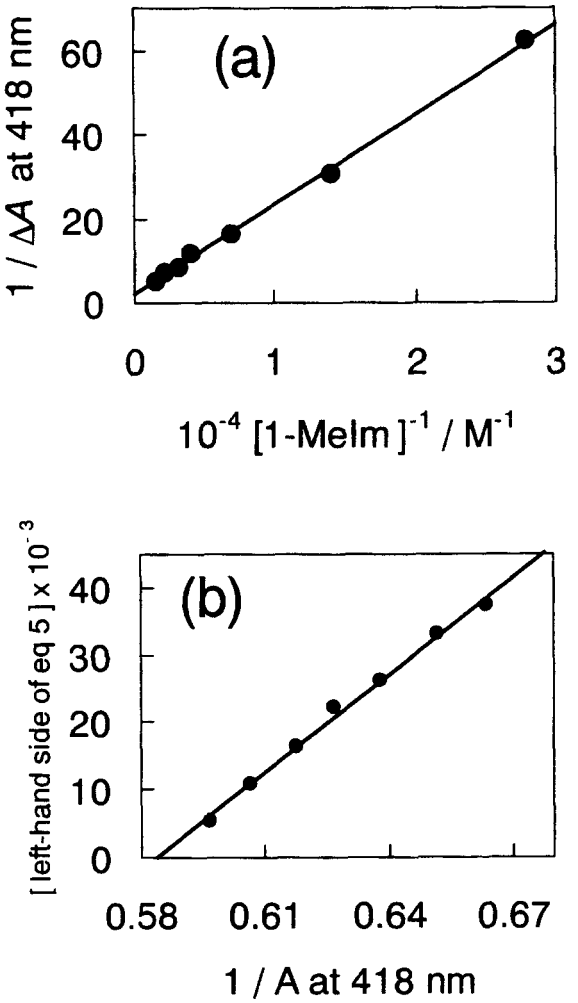

Fig. 4. Analysis of the 1-MeIm titration in Fig. 3. Parts (a) and (b) correspond to the results of (a) and (b) in Fig. 3, respectively.

of **1**·Cl, owing to improved solubility in cold organic solvent to allow us easier EPR observation in frozen glass. In the absence of 1-MeIm, as expected from the symmetry-lowering deformation in corrphycene, the chloro corrphycenaroiron(III) exhibited a somewhat rhombic high-spin spectrum with g = 6.57, 5.33, and 1.96 (Fig. 6). With addition of 0.5 molar amount of 1-MeIm, another set of rhombic high-spin signals appeared, although the new g-values are not accurately determined because of severe overlap of the two high-spin components. In the presence of four molar amounts of 1-MeIm, the low-spin signals at g = 2.46, 2.27, and 1.87 became exclusively dominant. The EPR transitions indicate the two-step behavior of the 1-MeIm coordination, consistent with the visible (Fig. 3) and NMR (Fig. 5) observations. We assigned the high- and low-spin states for the mono and bis 1-MeIm intermediates, respectively, on the basis of the EPR results.

1-Methylimidazole Binding to the Bromo and Iodo Complexes. According to the spectrochemical series of ligands,[28] the ligand-field splitting parameter varies in the order of $Cl^- > Br^- > I^-$, suggesting the weaker axial interac-

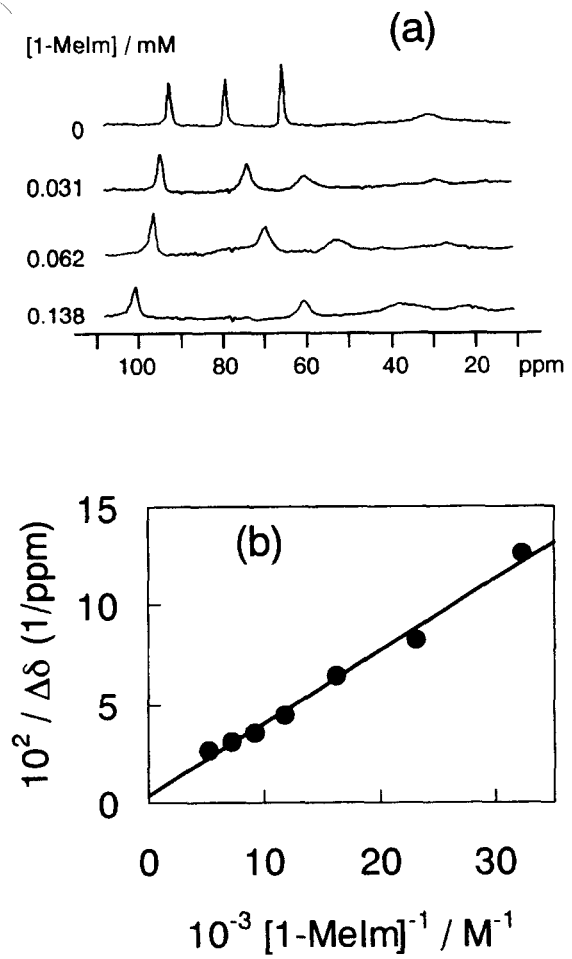

Fig. 5. Effect of 1-MeIm on the proton NMR spectrum of corrphycenatoiron(III) **1**·Cl. (a) In $CDCl_3$ at 20 °C and [**1**·Cl] = 1.0 mM. (b) Analysis of the methyl peak originally observed at 67.9 ppm in the absence of 1-MeIm. The binding constant $K_1 = 900 \pm 23$ M^{-1} was obtained.

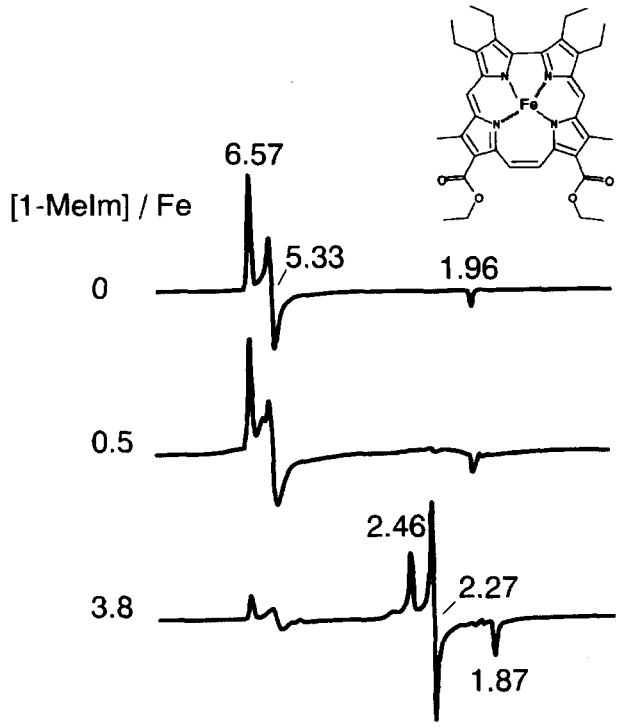

Fig. 6. Titration of 1-MeIm to the chloro corrphycenatoiron-(III), 0.5 mM, in $CHCl_3$–$C_6H_5CH_3$ (1 : 1) mixture as monitored with X-band EPR at 4.2 K. Formation of a high-spin intermediate is noted. Inset, structure of the corrphycenatoiron(III).

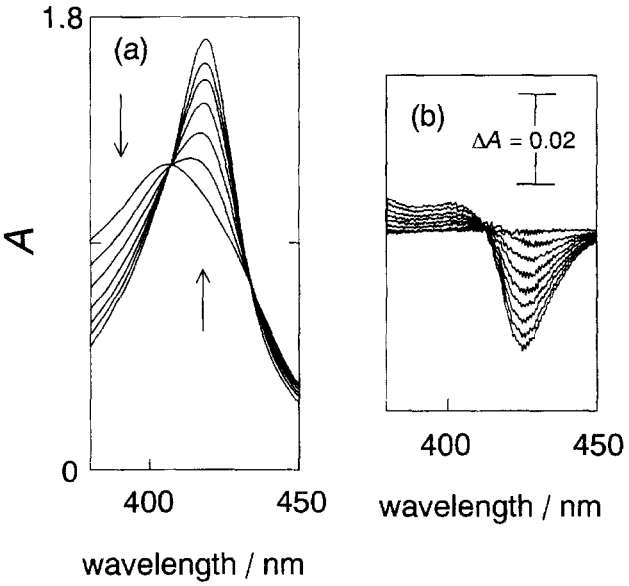

Fig. 7. Spectrophotometric titration of 1-MeIm to **1**·Br in $CHCl_3$ at 20 °C. (a) [1-MeIm] = 0 to 4.41 mM. Arrows indicate increase in 1-MeIm concentrations. (b) [1-MeIm] = 17.9 (base line) to 161.3 mM. The iron concentration is 13.1 μM in the two experiments.

tions in the bromo and iodo derivatives of corrphycenatoiron-(III). We examined the 1-MeIm coordination to **1**·Br and **1**·I to check if the anomaly in 1-MeIm ligation was amplified on weakening of the axial ligand-field. Figure 7 shows the Soret transition of **1**·Br during 1-MeIm binding. The 418-nm Soret developed accompanied with a set of clear isosbestic points at 407 and 433 nm below 5 mM of 1-MeIm. At high 1-MeIm concentrations over 18 mM, further changes accompanied with a poor isosbestic point at 412 nm were observed (Fig. 7). Although the second optical changes represent only ±2% of the total absorbance, they are absolutely reproducible and significant. Analyses of the two-step transition according to Eqs. 2 and 3 afforded $K_1 = 2.0 \times 10^4$ M^{-1} and $K_2 = 4.1$ M^{-1} for **1**·Br. Similar two-step spectral changes were observable for **1**·I with well-defined isosbestic points at 403 and 433 nm in the first step and poor isosbestic points around 393 and 422 nm in the second step. The ligation constants were $K_1 = 1.6 \times 10^4$ M^{-1} and $K_2 = 6.5$ M^{-1} for **1**·I. As for the corresponding porphyrins, the 1-MeIm binding proceeded in two steps. Analyses of the 1-MeIm-induced Soret transition with Eqs. 2 and 3 resulted in $K_1 = 84$ M^{-1} and $K_2 = 69$ M^{-1} for **2**·Br and $K_1 = 2.0 \times 10^3$ M^{-1} and $K_2 = 4.1$ M^{-1} for **2**·I. All of these results are incorporated in Table 1.

Discussion

Unique Accumulation of Mono 1-Methylimidazole Intermediate. The above results show that the coordination of 2-MeIm and Im to **1**·Cl proceeds with and without appreciable formation of the intermediate, respectively. Accumulation of mono 2-MeIm adduct with hindered iron(III)–*N*(2-MeIm) bond is well pronounced in porphyrinatoiron(III)[10,12] and crystal structure of the mono 2-MeIm adduct of octaethylporphyrinatoiron(III) has been resolved by Scheidt et al.[29] Absence of the mono Im adduct has been ascribed to the hydrogen bonding on the NH in Im ring[10,14] as well as the unhindered iron(III)–*N*(Im) bond. Present observations for corrphycene towards Im and 2-MeIm compare well with those reported for porphyrinatoiron(III) complexes[7–12] indicating that the fundamental coordination profiles of Im and 2-MeIm are just alike between corrphycenato- and porphyrinatoiron(III) complexes.

However, a potential difference exists between them in the reactivity against 1-MeIm. Little mono 1-MeIm adduct accumulates in porphyrin **2**·Cl as well as in regular porphyrinatoiron(III) derivatives[10–13] because the equilibrium constant K_1 is close to unity, reflecting an unhindered iron(III)–*N*(1-MeIm) bond. La Mar and Walker[30] reported indirect NMR evidence that a minor fraction of mono 1-MeIm adduct of tetraphenylporphyrinatoiron(III) is formed above 50 °C, and Deoff and Sweigart[13] claimed that the mono 1-MeIm species can be trapped only as an transient species during rapid mixing. In remarkable contrast to these circumstantiated results for porphyrinatoiron(III) complexes,[10–13] the visible spectrophotometry for **1**·Cl in Fig. 2 reveals that 1-MeIm, a typical unhindered imidazole, forms a stable mono 1-MeIm intermediate in appreciable amounts. The NMR and EPR observations in Figs. 5 and 6 provide support for the finding from the Soret spectral changes. With $K_1 = 930\ M^{-1}$ and $K_2 = 290\ M^{-1}$ for **1**·Cl in Table 1, the maximum fraction of the mono-1-MeIm species is calculated to be 0.46 at [1 − MeIm] = 1.5 mM, where the bis adduct fraction is only 0.20. The equilibrium constant $K_1 = 930\ M^{-1}$ by photometric titration well compares with $K_1 = 900\ M^{-1}$ from NMR under a much higher concentration of **1**·Cl. The two K_1 values from the discrete physical techniques are consistent, suggesting the reliability of the figure. The mono 1-MeIm complex may be either six-coordinate with 1-MeIm and chloride as axial ligands, or five-coordinate with one 1-MeIm and tightly associating chloride in the outer sphere. In view of the coordination structure for octaethylporphyrinatoiron(III) complexed with one 2-MeIm,[29] a five-coordination of 1-MeIm is a more likely possibility for our corrphycene compound. Although definitive assignment of the coordination number must await further analysis, the EPR in Fig. 6 allows us unambiguous assignment of high-spin state to the mono 1-MeIm intermediate.

First 1-Methylimidazole Ligation. Accumulation of an intermediate with a single unhindered 1-MeIm is a notable attribute of corrphycenatoiron(III). The stabilization of 1-MeIm adduct is expected to reflect the iron reactivity change in the deformed core. In the stepwise bis ligation of 1-MeIm to the corrphycenatoiron(III), two remarkable changes in coordination are expected, i.e. dissociation of the bound halide upon the first 1-MeIm ligation and subsequent movement of the iron atom into the plane on the second 1-MeIm binding. It is very likely that the first 1-MeIm molecule coordinates at the vacant sixth coordination site to induce out-of-plane displacement of the iron toward 1-MeIm with possible dissociation of the trans chloride. According to the X-ray analysis, corrphycene has a narrower central cavity than porphyrin.[2a,16] The narrower cavity could cause a shorter iron(III)–*N*(pyrrole) bond. This is indeed observed in chloro corrphycenatoiron(III). The X-ray analysis by the Vogel–Sessler groups[2c,16] demonstrated that iron(III)–*N*(pyrrole) bond, 2.056 Å in average in chloro octaethylcorrphycenatoiron(III), is slightly shorter than 2.063 Å in chloro octaethylporphyrinatoiron(III). A shorter iron(III)–*N*(pyrrole) bond is similarly expected for **1**·Cl. It is notable in the NMR spectra in Fig. 5 that the methyl signals appear at $\delta = 91.7$, 78.4, and 67.9 for **1**·Cl and at $\delta = 55.0$, 53.5, and 39.6 for **2**·Cl. According to the NMR analysis for high-spin porphyrinatoiron(III) complexes, peripheral methyl shifts reflect iron-spin transfer to the β-pyrrole carbons via σ bonds. Thus strength of equatorial bonds of the iron atom can be monitored with chemical shifts of the pyrrole methyls.[24] The larger methyl shifts in **1**·Cl in Fig. 5 thus suggest the stronger iron(III)–*N*(pyrrole) interactions in corrphycene, consistent with the narrower coordination hole. The stronger equatorial interactions in turn cause weakening of the axial iron(III)–Cl bond. The result that K_1 (**1**·Cl) > K_1 (**2**·Cl)[31] in 1-MeIm binding indicates a weaker iron(III)–Cl bond in **1**·Cl. The result that K_1 (**1**·Cl) > K_1 (**2**·Cl) in 2-MeIm binding in Table 1 suggests the same possibilities. We propose that the larger K_1 of 1-MeIm or 2-MeIm for **1**·Cl as compared with **2**·Cl thus comes from weaker axial interactions. Additional support for the present idea comes from the observations for other halogen derivatives. As the comparison among **1**·Cl, **1**·Br, and **1**·I in Table 1 indicates, substitution of chloride with weaker bromide or iodide[28] remarkably enhances K_1. A similar result in Table 1 that K_1(**2**·Cl)[31] < K_1(**2**·Br) < K_1(**2**·I) for 1-MeIm binding is also notable for porphyrin derivatives. It is therefore very likely that weakening of axial iron-halogen bond is a common denominator underlying corrphycene and porphyrin to enhance the first 1-MeIm ligation.

Second 1-Methylimidazole Ligation. Consideration for the second ligation process reveals another unique profile of corrphycene. Table 1 demonstrates that K_2 (**1**·Cl) < K_2 (**2**·Cl) in 2-MeIm ligation. We note a similar result in 1-MeIm binding that K_2 (**1**·Br) < K_2 (**2**·Br), although $\mathbf{K}_2$ (**1**·I) ≈ K_2 (**2**·I). If we assume a K_1 close to unity for the 1-MeIm coordination[31] to **1**·Cl, a relation K_2 (**1**·Cl) < K_2 (**2**·Cl) in the second 1-MeIm binding also holds. The smaller K_2 for **1** is another key feature to allow accumulation of the mono-1-MeIm intermediate. In going from the mono to bis 1-MeIm complexes, the iron changes from high- to low-spin (Fig. 6), and the low-spin iron comes into the corrphycene plane. Thus the second equilibrium constant K_2 is diagnostic of the iron

movement into corrphycene plane. According to the X-ray analysis,[2a,16] the central cavity in corrphycene is trapezoidal, in remarkable contrast with the square hole in porphyrin. In the deformed core, the four iron(III)–*N*(pyrrole) bonds are no longer orthogonal to each other. The geometric strain in the equatorial iron bonds may hold back accommodation of low-spin iron into the coordination hole to diminish the tendency for six-coordinate complex formation. The smaller K_2 values for corrphycene **1**, as compared with porphyrin **2** (Table 1), are thus rationalized by improper accommodation of the low-spin iron(III) due to the trapezoidal core deformation. It is notable in Table 1 that **1**·Cl exhibits a larger β_2 for Im than **2**·Cl. The result may be explained in terms of a possible increase in K_1 by easier chloride dissociation from **1**·Cl, as discussed in the above section, to mask the decrease in K_2 of Im ligation to **1**·Cl.

Biological Implication. Myoglobin reconstitution with synthetic hemin is susceptible to the molecular shape of porphyrin. Coupling with irregular hemin tends to cause the distal histidine ligation to the iron(III) to form a bis histidine complex, hemichrome. The phenomenon is typically found when tetrapropylhemin, a synthetic hemin with the meso-alkyl substituents, is introduced into the protein pocket.[32] In contrast, apomyoglobin successfully complexes with corrphycenatoiron(III)[5] without forming the hemichrome, despite the irregular molecular form of **1**. The corrphycene–substituted myoglobin, like native metmyoglobin, is an aquomet protein with the proximal imidazole and an iron-bound water molecule as axial ligands for the iron atom. Since corrphycenatoiron(III) exhibits remarkable ability to accumulate mono 1-MeIm, it is reasonably assumed that the native coordination structure achieved in corrphycene–reconstituted metmyoglobin[5] is the biological manifestation of the unique property of corrphycene.

We are indebted to Dr. J. L. Sessler (University of Texas at Austin) for his generous permission to access the Ph. D. dissertation of Dr. F. Zuniga-y-Rivero (University of Köln). This work was supported by grants-in-aid from the Ministry of Education, Science, Sports, and Culture (#10672031 and Frontier Research Program).

References

1 a) E. Vogel, *J. Heterocycl. Chem.*, **33**, 1461 (1996). b) J. L. Sessler and S. J. Weghorn, "Expanded, Contracted and Isomeric Porphyrins," Elsevier, New York (1997). c) J. L. Sessler, A. Gebauer, and E. Vogel, "The Porphyrin Handbook," Academic Press, New York (2000), Vol. 2, pp. 1—54.

2 a) J. L. Sessler, E. A. Brucker, S. J. Weghorn, M. Kisters, M. Schäfer, J. Lex, and E. Vogel, *Angew. Chem., Int. Ed. Engl.*, **33**, 2308 (1994). b) M. A. Aukauloo and R. Guilard, *New J. Chem.*, **18**, 1205 (1994).

3 H. Falk and Q.-Q. Chen, *Monatsh. Chem.*, **127**, 69 (1996).

4 S. Neya, K. Nishinaga, K. Ohyama, and N. Funasaki, *Tetrahedron Lett.*, **39**, 5217 (1998).

5 S. Neya, N. Funasaki, H. Hori, K. Imai, S. Nagatomo, T. Iwase, and T. Yonetani, *Chem. Lett.*, **1999**, 989.

6 M. S. Hargrove, A. J. Wilkinson, and J. S. Olson, *Biochemistry*, **35**, 11293 (1996).

7 M. Momenteau, *Biochim. Biophys. Acta*, **304**, 814 (1973).

8 T. H. Davies, *Biochim. Biophys. Acta*, **329**, 108 (1973).

9 C. L. Coyle, P. A. Rafson, and E. H. Abbott, *Inorg. Chem.*, **12**, 2007 (1973).

10 F. A. Walker, M.-W. Lo, and M. T. Ree, *J. Am. Chem. Soc.*, **98**, 5552 (1976).

11 R. F. Pasternack, B. S. Gillies, and J. R. Stahlbush, *J. Am. Chem. Soc.*, **100**, 2613 (1978).

12 T. Yoshimura and T. Ozaki, *Bull. Chem. Soc. Jpn.*, **52**, 2268 (1979).

13 M. M. Doeff and D. A. Sweigart, *Inorg. Chem.*, **21**, 3699 (1982).

14 G. A. Tondreau and D. A. Sweigart, *Inorg. Chem.*, **23**, 1060 (1984).

15 C. T. Brewer and G. A. Brewer, *Inorg. Chem.*, **26**, 3240 (1987).

16 F. Zuniga-y-Rivero, Ph. D. Dissertation, University of Köln, Germany (1998).

17 S. Neya, N. Funasaki, N. Igarashi, A. Ikezaki, T. Sato, K. Imai, and N. Tanaka, *Biochemistry*, **37**, 5487 (1998).

18 D. Adler, F. Longo, F. Kampas, and J. Kim, *J. Inorg. Nucl. Chem.*, **32**, 2443 (1970).

19 C. Maricondi, W. Swift, and D. K. Straub, *J. Am. Chem. Soc.*, **91**, 5205 (1969).

20 D. D. Perrin and W. L. F. Armarego, "Purification of Laboratory Chemicals," 3rd ed., Pergamon Press, New York (1988).

21 H. A. Benesi and J. H. Hildebrand, *J. Am. Chem. Soc.*, **71**, 2703 (1949).

22 F. J. C. Rossotti and H. Rossotti, "The Determination of Stability Constants," McGraw-Hill, New York (1961), p. 277.

23 S. Neya, I. Morishima, and T. Yonezawa, *Biochemitry*, **20**, 2610 (1981).

24 G. N. La Mar and F. A. Walker, "The Porphyrins," Academic Press, New York (1979), Vol. 4, pp. 61—157.

25 The NMR transition observed during addition of 1-MeIm suggests that the 91.7-ppm signal is from 11- and 18-methyls on the corrphycene ring, and the 78.4- and 67.9-ppm peaks come from the remaining four methyls.

26 F. Takahashi and N. C. Li, *J. Am. Chem. Soc.*, **88**, 1117 (1996).

27 S. Neya and I. Morishima, *Biochemistry*, **19**, 258 (1980).

28 D. F. Shriver, P. W. Atkins, and C. H. Langford, "Inorganic Chemistry," 2nd ed, Oxford University Press, Oxford (1994), p. 246.

29 W. R. Scheidt, D. K. Geiger, Y. J. Lee, C. A. Reed, and G. Lang, *J. Am. Chem. Soc.*, **107**, 5693 (1985).

30 G. N. La Mar and F. A. Walker, *J. Am. Chem. Soc.*, **94**, 8607 (1972).

31 The direct bis coordination of 1-MeIm to **2**·Cl (Table 1) indicates that $K_1 \ll K_2$. In view of the reported results[10,12,13] and the electron-withdrawing ethoxycarbonyl groups in **2**, a K_1 close to unity is practical approximation in the 1-MeIm ligation to **2**·Cl.

32 S. Neya and N. Funasaki, *Biochim. Biophys. Acta*, **952**, 150 (1988).